Doping properties of monoclinic BiVO_{4} studied by first-principles density-functional theory

Wan-Jian Yin, Su-Huai Wei, Mowafak M. Al-Jassim, John Turner, and Yanfa Yan

Doping properties of monoclinic BiVO$_4$

Wan-Jian Yin, Su-Huai Wei, Mowafak M. Al-Jassim, John Turner, and Yanfa Yan*

National Renewable Energy Laboratory, Golden, CO 80401

ABSTRACT

The intrinsic and extrinsic doping properties of BiVO$_4$, i.e., the formation energies and transition energy levels of defects and impurities, have been studied systematically by first-principles density-functional theory. We find that for doping caused by intrinsic defects, O vacancies are shallow donors and Bi vacancies are shallow acceptors. However, these defects compensate each other and can only lead to moderate *n*-type and *p*-type conductivities at Bi-rich and O-rich growth conditions, respectively. To obtain BiVO$_4$ with high *n*-type and *p*-type conductivities, which are required for forming ohmic contacts, extrinsic doping using foreign impurities is necessary. Our results reveal that Sr, Ca, Na, and K atoms on Bi sites are very shallow acceptors and have rather low formation energies. The calculated Fermi-level pinning positions predict that doping of these impurities under oxygen-rich growth conditions should result in outstanding *p*-type conductivity. Substitutional Mo and W atoms on V sites are very shallow donors and have very low formation energies. Fermi-level pinning position calculations expect the doping of Mo and W under oxygen-poor growth conditions to produce excellent *n*-type conductivity. Also discussed is the dependence of formation energies and transition energies of defects on the atomic size and atomic chemical potential trends.

* Corresponding author: yanfa.yan@nrel.gov

I.   Introduction

Use of sunlight and semiconductors to split water to generate hydrogen provides a viable way for producing renewable and storable energies. It has attracted great attention since the early realization of solar-driven water splitting using TiO_2 in the 1970s [1]. However, the large bandgap of TiO_2 (~3 eV) makes it photoelectrochemically (PEC) active only in the ultraviolet (UV) range, which is a small portion (<5%) of sunlight [2]. For effective use of sunlight, the ideal bandgap of the semiconductor absorbers should be around 2.0 eV. Metal oxides are considered as potential candidates for PEC water splitting because of their resistance to oxidization and possible stability in aqueous solutions. Therefore, searching for metal oxide semiconductors with appropriate bandgaps has been one of the research focuses in the field of PEC water splitting [2-8]. Among the large number of metal oxides proposed, $BiVO_4$ has shown very promising performance [9-12]. The monoclinic $BiVO_4$ has a direct bandgap of 2.4-2.5 eV, good optical absorption properties, and reasonable band edge alignment with respect to H/H_2O and O/H_2O redox potentials [12,13].

For optimal solar to hydrogen conversion, the optical absorber layers (the semiconductors used) should have moderate p-type or n-type conductivities to minimize photo-generated carrier recombination. For best carrier collection and transportation, the absorber layers should also be able to form ohmic contacts with contact materials, which requires semiconductors with the ability to be doped highly p-type or n-type in terms of electrical conductivity. Furthermore, doping (intrinsic or extrinsic) creates the needed built-in electrical fields near the semiconductor/liquid interfaces to separate photon-generated carriers. Therefore, the doping properties of the semiconductors used for PEC water splitting critically affect device performance. Recently, Yao et al. [14] found experimentally that the PEC activity of $BiVO_4$ for

2

water oxidation or organic compound degradation was remarkably enhanced by Mo doping. They further found that $Ca_xBi_{1-x}V_{1-x}Mo_xO_4$ had a great variable range for Ca and Mo solubility [15]. Similar effects were also found in $Ca_xBi_{1-x}V_{1-x}W_xO_4$ by Sameera et al. [16]. Sayama et al. [9] showed that Ag ion treatment of $BiVO_4$ significantly enhances the PEC response. The incorporation of Na [17,18], Eu [19], Dy [20], Pd [21], and Si [22] had also been reported to enhance PEC performance of $BiVO_4$. It is expected that the mechanism of the effects could be different for various impurity incorporation. Some of the incorporated impurities may act as catalysts, whereas others may simply affect the crystal growth or may alter the formation of defects and subsequently the doping properties. To explore the optimal performance of $BiVO_4$, it is necessary to perform a systematic study of the defect physics in this compound, which can provide a fundamental understanding on what dopants could be potential shallow acceptors or donors, what defects could be harmful to PEC response, what growth conditions may promote the formation of desirable defects, and what growth conditions may suppress the formation of harmful defects. This information may provide useful guidance for designing appropriate growth approaches for improved PEC performance and insights for understanding experimental results obtained.

In this paper, we systematically study the doping properties, for both intrinsic and extrinsic doping, of $BiVO_4$ and understand how they may impact the conductivity using first-principle density-functional theory (DFT). We calculate the transition energies and formation energies of intrinsic and impurity defects and Fermi-level pinning positions. We find that intrinsic doping can only lead to moderate n-type and p-type conductivities at Bi-rich and O-rich growth conditions, respectively, although O vacancies are very shallow donors and Bi vacancies are very shallow acceptors. Excellent n-type and p-type conductivities, which are required for forming

3

ohmic contacts, can only be obtained through extrinsic doping. Sr, Ca, Na, and K atoms on Bi sites are found to be very shallow acceptors and have rather low formation energies. Therefore, the doping of these impurities is predicted to result in outstanding *p*-type conductivity. Substitutional Mo and W atoms on V sites are very shallow donors and have very low formation energies. Thus, doping of Mo and W is expected to produce excellent *n*-type conductivity. We further find that formation energies and transition energies of defects depend on the atomic size and atomic chemical potential trends.

II.   Computational Methodology

2.1 Computational methods

The calculations were performed using the DFT as implemented in the VASP code [23] using the standard frozen-core projector augmented-wave (PAW) method [24]. For the exchange-correlation functional, the generalized gradient approximation (GGA) of Perdew et al. [25] was used. The cut-off energy for basis functions is 400 eV. The crystal structure of $BiVO_4$ considered in this work is in the base-centered monoclinic phase (space group 15, C_{2h}^6), which has been confirmed experimentally to exhibit good PEC performance. The k-points mesh for the 96-atom $BiVO_4$ (2a, b, 2c of conventional cell) host supercell is 2×3×3. Our calculated lattice parameter for a conventional cell is a = 7.32 Å, b= 11.79 Å, c= 5.17 Å, β= 134.90°, which are in good agreement with previous theoretical results [12].

2.2 Formation enthalpy of defects

We used the mixed scheme for formation energy calculation. This method combines the advantages of the special k-point (more accurate for total energies) and Γ-point-only approach (more accurate for defect levels) [26,27], and it has been successfully applied to various semiconductors [28-30]. The formation energy of a defect α with charge state q, $\Delta H_f(\alpha,q)$, depends on the position of Fermi level, E_F [relative to the valence-band maximum (VBM)], transition level $\varepsilon(0/q)$, and chemical potential μ_i, and can be described as:

$$\Delta H_f(\alpha,q) = \Delta H_f(\alpha,0) - q\varepsilon(0/q) + qE_F \ , \tag{1}$$

where $\Delta H_f(\alpha,0)$ is defined as:

$$\Delta H_f(\alpha,0) = E(\alpha,0) - E(bulk,0) + \sum_i n_i(E_i+\mu_i) \ . \tag{2}$$

Here, $E(\alpha,0)$ and $E(bulk,0)$ are total energies of supercells with a neutral defect and without defect, respectively, and E_i and μ_i are energy per atom of elemental phase and its chemical potential, respectively. The transition level $\varepsilon(0/q)$ is defined as the Fermi level at which the neutral defect has the same formation energy as the defect with charge state q. For an acceptor (q<0), the transition level measures how deep/shallow the defect level is. It contains two parts: single-electron defect level at Γ point and structural and Coulomb relaxation energy. With respect to VBM, the transition level can then be written as:

$$\varepsilon(0/q) = [\varepsilon^\Gamma_D (\alpha,0) - \varepsilon^\Gamma_{VBM} (bulk,0)] + \{E(\alpha,q) - [E(\alpha,0) - q\varepsilon^k_D (\alpha,0)]\}/(-q) \ . \tag{3}$$

The former single-electron defect level is calculated using only Γ point, and the latter structural and Coulomb relaxation is calculated using special k points, which is required by their individual physical meaning. Because the $\varepsilon^\Gamma_D (\alpha,0)$ and $\varepsilon^\Gamma_{VBM} (bulk,0)$ are eigenvalues in two different systems, the 1s core levels of O atoms far away from defects in the two systems are aligned. For

donor levels (q>0), the electron ionization energy is used to measure how deep/shallow the defect level is. The electron ionization energy, which is referenced to the conduction-band minimum (CBM), can be written as:

$$\varepsilon(0/q) = [\varepsilon^\Gamma_{CBM}(bulk,0) - \varepsilon^\Gamma_D(\alpha,0)] + \{E(\alpha,q) - [E(\alpha,0) - q\varepsilon^k_D(\alpha,0)]\}/q \ . \tag{4}$$

2.3 Chemical potentials

Under thermal equilibrium growth conditions, the steady production of host material, BiVO$_4$, should satisfy the following equation [26,27]:

$$\mu_{Bi} + \mu_V + 4\mu_O = \Delta H_f(BiVO_4) = -13.95 \text{ eV} \ , \tag{5}$$

where μ_{Bi}, μ_V, and μ_O are chemical potentials of Bi, V, and O source, respectively, and ΔH_f is the formation energy for BiVO$_4$ per formula. To avoid the precipitation of source elements, μ_{Bi}, μ_V, and μ_O must satisfy

$$\mu_{Bi} < 0, \ \mu_V < 0, \ \mu_O < 0 \ , \tag{6}$$

which is smaller than the bulk Bi, V, and O$_2$ gas, respectively. To avoid the formation of secondary phases (such as Bi$_2$O$_3$, VO$_2$, and V$_2$O$_5$), μ_{Bi}, μ_V, and μ_O must satisfy further constraints:

$$2\mu_{Bi} + 3\mu_O < \Delta H_f(Bi_2O_3) \tag{7}$$

$$\mu_V + 2\mu_O < \Delta H_f(VO_2) \tag{8}$$

$$2\mu_V + 5\mu_O < \Delta H_f(V_2O_5) \ . \tag{9}$$

Considering Eqs. (5)-(9), the accessible range for μ_{Bi}, μ_V, and μ_O is limited and is illustrated as the red shaded area in Fig. 1. As shown in Eqs. (1) and (2), the calculated formation energies of charged defects depend sensitively on the selected values for μ_{Bi}, μ_V, and μ_O, and the Fermi-level positions. Here, we present calculated values at two representative chemical potential points labeled as A (Bi rich/O poor) and B (O rich) in Fig. 1. The exact value of chemical potentials at points A and B are (0, -2.08, -2.97 eV) and (-4.41, -9.54, 0 eV) for μ_{Bi}, μ_V, μ_O, respectively. The formation energies at other achievable chemical potentials can be obtained from Eqs. (1) and (2). For impurity doping, the chemical potentials of impurities also need to satisfy other constraints to avoid the formation of impurity-related phases. For example, for Mo doping, the chemical potential of Mo is constrained by $\mu_{Mo} < 0$ and $\mu_{Mo} + 3\mu_O < \Delta H_f(MoO_3) = -8.92$ eV. These lead to $\mu_{Mo} < -0.02$ eV. In this case, the $\mu_{Mo} = -0.02$ eV is used for the calculation of formation energy for Mo-related defects.

III. Results and Discussion

3.1 Properties of bulk BiVO$_4$

In the monoclinic phase of BiVO$_4$, each Bi atom has 8 O coordinates and each V atom has 4 O coordinates. In this oxide, the ionization state of Bi is 3+ and it has lone pair $6s^2$ electrons [31,32]. As a result, BiVO$_4$ exhibits unique electronic and structural properties. The calculated band structure and site-projected density of states (DOS) of BiVO$_4$ are shown in Figs. 2 and 3. The calculated GGA bandgap for BiVO$_4$ is 2.06 eV, which is about 0.44 eV smaller than the experimental value. The bandgap is direct with both VBM and conduction band minimum (CBM) located at A point. The VBM at A points is about 0.3 eV higher than that at Γ point. The valence band are mainly composed of the bonding states of O 2p-V 3d and O 2p-Bi 6p and the

7

bottom conduction bands are mainly composed of the antibonding states. The lone pair Bi 6s orbital also couples with O 2p orbital and produce filled antibonding states near VBM. Such coupling makes BiVO$_4$ a direct bandgap at A point not at Γ point as in conventional semiconductors. For supercells calculations, the states at A point fold to Γ point. Therefore, for defect level calculations, only Γ point was considered.

3.2 Intrinsic defects

Intrinsic defects considered in this study include: Bi$_{vac}$ (Bi vacancy), V$_{vac}$ (V vacancy), O$_{vac}$ (O vacancy), Bi$_V$ (Bi on V site), V$_{Bi}$ (V on Bi site), Bi$_{int}$ (Bi interstitial), V$_{int}$ (V interstitial), and O$_{int}$ (O interstitial). Because of their large formation energies, cation/anion antisites, such as Bi or V on O site and O on Bi or V site, are not discussed in this study. From single particle energy point of view, Bi$_{vac}$, V$_{vac}$, Bi$_V$, and O$_{int}$ should be acceptor-like defects, whereas O$_{vac}$, V$_{Bi}$, Bi$_{int}$, and V$_{int}$ should be donor-like defects. The calculated transition energies for these defects are listed in Table I. It is seen that O$_{vac}$, V$_{Bi}$, V$_{int}$, and Bi$_{int}$ are donor-like defects, but only O$_{vac}$ is a shallow donor. Its (0/+2) transition level is even above the CBM of BiVO$_4$. This unusual characteristic is due to the large size and chemical mismatch of cation Bi and V [33]. Bi$_{vac}$, V$_{vac}$, Bi$_V$, and O$_{int}$ are acceptor-like defects, but only Bi$_{vac}$ is a shallow acceptor. Bi is 3+ in BiVO and therefore it has 6s^2 lone pair electrons. These lone pair electrons couple with O 2p electrons forming occupied antibonding states. Therefore the Bi-O bonding is much weaker than the V-O bonding. As a result, we find that the creation of a Bi$_{vac}$ does not cause significant lattice relaxation around the vacancy site. The relaxation leads to only 0.04 Å reduction on V-O bond length for V and O atoms around the vacancy site. Such small relaxations cause very small perturbation on the valance states and therefore lead to a shallow acceptor level. The formation of shallow donors (O$_{vac}$) or shallow acceptors (Bi$_{vac}$) is responsible for the *n*-type or *p*-type

8

conductivities. However, the formation of the deep donors and acceptors usually compensate the conductivities and often behave as harmful photo-generated carrier traps.

The conductivity of a semiconductor depends not only on the transition energy levels of donor and acceptors, but also on their formation energies. To predict the conductivity of $BiVO_4$ by intrinsic defects, the Fermi level pinning positions should be calculated. Figures 4(a) and 4(b) show the calculated formation energies for intrinsic defects as functions as Fermi levels at chemical potential points A and B, respectively. As mentioned above, our calculated GGA bandgap for $BiVO_4$ (2.06 eV) is about 0.44 eV smaller than the experimental value, 2.5 eV. For this small difference, we have simply applied a scissor operation to correct the bandgap. The transition levels referred to VBM (for acceptors) or CBM (for donors) are kept unchanged. The formation energies for Bi_{int} are not shown because they are too high as compared to other defects. The high formation energies of Bi_V and V_{Bi} could be explained by the large chemical and ionic-size difference between Bi^{3+} and V^{5+}. The ionic radii of cations considered in this paper are listed in Table II. In general, the formation energies of donors are much lower at the A (Bi rich/O poor) condition than at the B (O rich) condition, and it is opposite for the formation energies of acceptors. Bi_{vac} has a lower formation energy than V_{vac} due to Bi-O antibonding coupling. Under the A condition, the formation energy of O_{vac} is very low, meaning that *n*-type conductivity can be realized by the formation of O_{vac}. However, the Fermi level is pinned to be at ~0.35 eV below CBM by the formation of Bi_{vac}, as indicated by the dashed black line in Fig. 4(a). Under the B condition, the formation of Bi_{vac} is able to produce *p*-type conductivity, but the Fermi level is pinned to be at ~0.55 eV above VBM by the formation of O_{vac}, as indicated by the dashed black line Fig. 4(b). Our results therefore suggest that to obtain *n*-type conductivity, $BiVO_4$ should be synthesized under Bi rich/O-poor conditions. To produce *p*-type conductivity, $BiVO_4$ should be

grown under O-rich conditions. However, without external doping, BiVO$_4$ with only moderate *n*-type or *p*-type conductivities may be produced due to Fermi-level pinning. For PEC absorbers, a moderate conductivity is just what it needs.

3.3 Group I element doping

For doping by group I elements, we have considered Li, Na, and K. These impurities can be at either interstitial sites or substitutional Bi or V sites. Therefore, nine different point defects— Li$_{Bi}$, Li$_V$, Li$_{int}$, Na$_{Bi}$, Na$_V$, Na$_{int}$, K$_{Bi}$, K$_V$, and K$_{int}$—have been included in our calculation. The calculated transition energies are summarized in Table III. It is seen that at interstitial sites, Li, Na, and K are all shallow donors. These results are understandable, because as mentioned above, the CBM of BiVO$_4$ is mainly derived from V 3d orbital and it is much lower in energy than the valence *s* orbitals of Li, Na, and K. At substitutional sites, Li, Na, and K are acceptors. However, they are much shallower at Bi sites than at V sites. This can be qualitatively understood as the following. The valence band is mainly derived from O 2p orbital. If a dopant has smaller perturbation on the valence band, it will have shallower acceptor levels. In BiVO$_4$, the average Bi-O bond length is 2.48 Å, whereas the average V-O bond length is 1.74 Å. Thus, cation substitution at Bi sites should lead to much smaller perturbation on the valence band than the substitution at V sites. Consequently, substitutional Li, Na, and K should have much shallower transition levels at Bi sites than at V sites. Furthermore, as we discussed above, the remove of Bi does not cause significant lattice relaxation. The contribution from geometry relaxations is not expected to play important role.

As mentioned above, the doping ability also depends on defect concentration or the formation energies. Figures 5(a) and 5(b) show the calculated formation energies as functions of

the Fermi levels for Li-, Na-, and K-related defects at chemical potential points A (Bi rich/O-poor condition) and B (O-rich condition), respectively. The chemical potentials of Li, Na, and K are chosen to avoid the formation of Li_2O, Na_2O, and K_2O and elemental metals. The derived upper-limit chemical potentials for Li, Na, and K are -1.60, -0.71, and -0.32 eV at point A condition and -3.09, -2.20, and -1.80 eV at point B condition. Because the formation of intrinsic defects may compensate the extrinsic doping, the lowest formation energies of intrinsic defects are also shown as the dashed lines in Fig. 5. At point A condition, substitutional Li, Na, and K have much lower formation energies at Bi sites than at V sites, in part because they are shallower acceptors at Bi sites than at V sites. Interstitial Li, Na, and K also have small formation energies. Thus, the compensation between interstitial dopants and substitutional dopants at Bi sites pins the Fermi levels. For Li doping, the Fermi level is pinned at ~0.6 eV below the CBM, as indicated by the green dashed line in Fig. 5(a). For Na, the Fermi level is pinned at ~1.2 eV below the CBM. For K doping, the Fermi level will be pinned at 1.9 eV below the CBM. Thus, at point A condition, group-I elements doping cannot lead to good *p*-type or *n*-type conductivities. The situation becomes very different at point B condition. In this case, the acceptors, Na_{Bi} and K_{Bi}, have much lower formation energies than their interstitial counterparts. The Fermi levels are pinned at ~0.35, ~0.1, and ~0.2 eV above the VBM, for Li, Na, and K doping, respectively. Thus, excellent *p*-type conductivities may be realized by Na and K doping at O-rich growth conditions. The formation energy for Li_{Bi} is larger than that for Na_{Bi} and K_{Bi}. The formation energy trend may be understood qualitatively by the ionic radii of Li^+, Na^+, and K^+ as listed in Table II. Because Li_{Bi}, Na_{Bi}, and K_{Bi} have very similar transition energies, the formation energy difference is likely attributed to the lattice distortion caused by cation substitutions, or the size difference between the substitutional ion and Bi^{3+}. The radii of Na^+

(0.95 Å) and K^+ (1.33 Å) are closer to that of Bi^{3+} (1.11 Å) than Li^+ (0.68 Å), consistent with the calculated formation energy trend. Duraisamy and Ramanan [17] synthesized the $Na_{x/2}Bi_{1-x/2}Mo_xV_{1-x}O_4$ with the x variable from 0 to 1, and a homogenous phase could be seen by scanning electron microscopy. They confirmed that Na favors Bi sites more than other sites such as interstitial sites and V sites.

3.4 Group II element doping

For doping by group-II elements, we have considered Mg, Ca, and Sr in group IIA and Zn in group IIB and three different defect configurations (substitution on Bi site, substitution on V site, and interstitial site). Therefore, there are 12 different point defects—Mg_{Bi}, Mg_V, Mg_{int}, Ca_{Bi}, Ca_V, Ca_{int}, Sr_{Bi}, Sr_V, Sr_{int}, Zn_{Bi}, Zn_V, and Zn_{int}—considered in this study. The calculated transition energies for all these defects are listed in Table IV. Group-II elements are acceptors at both Bi and V sites. However, their transition energies are much shallower at Bi sites than at V sites. As in the reason for group-I elements, substitution at Bi sites causes a smaller perturbation on the valence band than at V sites due to the large impurity-O bond length. It is seen that these substitutions at Bi sites lead to very shallow acceptors.

The calculated formation energies as a function of Fermi energy for the 12 defects at point A and point B conditions are shown in Figs. 6(a) and 6(b), respectively. The chemical potentials of Mg, Ca, Sr, and Zn are chosen to avoid the formation of MgO, CaO, SrO, and ZnO and elemental metals. The derived upper-limit chemical potentials for Mg, Ca, Sr, and Zn are -3.21, -3.68, -3.09, and -0.51 eV at point A condition and -6.18, -6.65, -6.06, and -3.48 eV at point B condition, respectively. The lowest formation energies of intrinsic defects are also shown as the dashed lines. Similar to doping of group-I elements, good *n*-type conductivities cannot be

realized under any growth conditions due to donor-acceptor compensation. The *n*-type conductivities induced by group-II elements should be even worse than the intrinsic materials, as indicated by the black dashed line in Fig. 6(a). However, both Ca and Sr at Bi sites can lead to outstanding *p*-type conductivity. Ca_{Bi} and Sr_{Bi} have transition energies smaller than 0.1 eV and have very small formation energies under O-rich growth conditions. Though Mg_{Bi} and Zn_{Bi} have even shallower transition energies than Ca_{Bi} and Sr_{Bi}, they have higher formation energies (about 1 eV) than Ca_{Bi} and Sr_{Bi} because the radii of Ca^{2+} (0.99 Å) and Sr^{2+} (1.13 Å) are closer to that of Bi^{3+} (1.11 Å) than Zn^{2+} (0.74 Å) and Mg^{2+} (0.65 Å) (see Table II). Thus, Mg_{Bi} and Zn_{Bi} may be compensated by O_{vac}, as shown in Fig. 6(b). Therefore, for Ca and Sr doping at O-rich growth condition, the Fermi level is limited by their transition energies (0.1 eV above VBM), but not by pinning from the formation of other compensating defects. Therefore, Ca and Sr doping are expected to be excellent candidates for *p*-type doping of $BiVO_4$. It is therefore not surprising that $Ca_xBi_{1-x}V_{1-x}Mo_xO_4$ and $Ca_xBi_{1-x}V_{1-x}W_xO_4$ could be formed easily [15,16]. Our results suggest that $Sr_xBi_{1-x}V_{1-x}Mo_xO_4$ and $Sr_xBi_{1-x}V_{1-x}W_xO_4$ should also exist and exhibit good PEC performance.

3.5 Group IVB element doping

For doping by group-IVB elements, we have considered Ti, Zr, and Hf and three different configurations (substitution on Bi site, substitution on V site, and interstitial site). Therefore, there are nine different point defects—Ti_{Bi}, Ti_V, Ti_{int}, Zr_{Bi}, Zr_V, Zr_{int}, Hf_{Bi}, Hf_V, and Hf_{int}. The calculated transition energies for these defects are listed in Table V. Ti_{Bi}, Zr_{Bi}, and Hf_{Bi} are donors. Because Zr $4d^24s^2$ and Hf $5d^26s^2$ atomic orbitals have higher energy than Ti $3d^24s^2$, Zr_{Bi} and Hf_{Bi} are shallower donors than Ti_{Bi}. Ti_V, Zr_V, and Hf_V are acceptors with transition energies about 0.2 eV above the VBM.

Our calculated formation energies as a function of Fermi level for the group-IVB elements at point A and point B conditions are shown in Figs. 7(a) and 7(b), respectively. The chemical potentials of Ti, Zr, and Hf are chosen to avoid the formation of TiO_2, ZrO_2, and HfO_2 and their elemental metals. The derived upper-limit chemical potentials for Ti, Hf, and Zr are -4.08, -5.43, and -6.02 eV at point A condition and -10.02, -11.37, and -11.96 eV at point B condition, respectively. The interstitial group-IVB elements can only exist in heavily doped p-type $BiVO_4$ due to large formation energies. Hf_V and Zr_V have higher formation energies than Ti_V because the ionic radius of Ti^{4+}(0.68 Å) is closer to the radius of V^{5+} (0.52 Å) than Zr^{4+} (0.79 Å) and Hf^{4+} (0.78 Å). Due to the same reason, Hf_{Bi} and Zr_{Bi} have smaller formation energies than Ti_{Bi}. At point A condition [Fig. 7(a)], doping of group-IVB elements would mostly form n-type conductivity. For Ti doping, the n-type conductivity is contributed by O_{vac} and the Fermi level will be pinned at ~0.6 eV below the CBM by the formation of O_{vac} and Ti_V. Thus, Ti doping will reduce the n-type conductivity induced by O_{vac}. For Zr and Hf doping, the Fermi levels are pinned at about 0.2 eV below the CBM, by the formation of Zr_{Bi} and Bi_{vac} and Hf_{Bi} and Bi_{vac}. At point B conditions [Fig. 7(b)], doping of group-IVB elements will mostly form p-type $BiVO_4$. For Ti doping, the Fermi level is pinned at about 0.4 eV above the VBM by the formation of Ti_V and O_{vac}. For Zr and Hf doping, the Fermi levels are pinned at about 0.7 eV above the VBM by the formation of Bi_{vac} and Zr_{Bi} and Hf_{Bi}. The holes are provided by the intrinsic defect, Bi_{vac}, and Zr_{Bi} and Hf_{Bi} are compensators.

3.6 Group VIB element doping

For doping by group VIB elements, we have considered Cr, Mo, and W and three different defect configurations (substitution on Bi site, substitution on V site, and interstitial site). Therefore, there are nine different point defects—Cr_{Bi}, Cr_V, Cr_{int}, Mo_{Bi}, Mo_V, Mo_{int}, W_{Bi}, W_V,

and W_{int}—considered in the calculation. The calculated transition energies for these defects are listed in Table VI. All these defects are donors. Among them, the shallowest donor is W_V, whose transition level is 0.01 eV below the CBM. Mo_V is the second-shallowest donor with transition energy of 0.04 eV below the CBM. Therefore, W_V and Mo_V are potential donors for realizing good *n*-type conductivities. It should be noted that to predict accurately the levels of 3*d* transition metals such as Cr doped system, Coulomb interaction described by LDA+U is often required. The level calculated by LDA+U is usually deeper than that calculated by GGA. However, because GGA calculation already found that Cr_{Bi}, Cr_V, and Cr_{int} are very deep levels, we did not calculate their levels using LDA+U in this work.

The calculated formation energies as a function of Fermi energy for these defects at point A and B conditions are shown in Figs. 8(a) and 8(b), respectively. The chemical potentials for Cr, Mo, and W are chosen to avoid the formation of CrO_3, MoO_3, and WO_3 and their elemental metals. The derived upper-limit chemical potentials for Cr, Mo, and W are 0, -0.02, and -1.30 eV at point A condition and -7.46, -8.92, and -10.20 eV at point B condition, respectively. The dashed lines indicate the lowest formation energies of intrinsic defects. Because all defects related to group-VIB elements are donors, charge compensation will only come from the formation of intrinsic defects. Without considering charge transfer between the defects and Fermi reservoir, the group-VIB elements have lower formation energies at V sites than at Bi sites due to better ionic size matching (see Table II). At point A growth condition, Mo_V is the most promising donor. For Mo doping, the Fermi level is limited by its transition level, which is only 0.04 eV below the CBM. Because of no Fermi level pinning caused by the formation of compensating defects, Mo doping is able to produce excellent *n*-type conductivity under Bi-rich/O-poor growth condition. For W doping, the Fermi level is pinned at ~0.3 eV below the

CBM by the formation of Bi_{vac}. Thus, for *n*-type doping, W is not as good as Mo, although W_V is shallower than Mo_V. Under point B (Bi-poor/O-rich) condition, group-VIB elements do not lead to good *n*-type doping due to the compensation from Bi_{vac}.

3.7 Substitution defects C_O, N_O, and F_O

The impurities discussed in the above calculation are mostly on cation sites. On the other hand, *p*-type and *n*-type doping of metal oxides may also be realized by introducing impurities to O sites [36-46]. In this case, C, N, and F are the most considered impurities. Because interstitials of these impurities usually have large formation energies, we will only consider substitutional defects, C_O, N_O, and F_O.

N_O is a single acceptor with calculated transition energy of 0.26 eV above the VBM, which is shallower than N_O in other metal oxides, such as ZnO and SnO. The reason can be attributed in part to the high VBM of $BiVO_4$ contributed by Bi 6s lone pair states. C_O is a double acceptor with calculated transition energies of 1.02 and 1.05 eV above the VBM. F_O is a good donor with calculated transition energy of 0.09 eV below the CBM. The calculated formation energies as a function of Fermi levels for C_O, N_O, and F_O at point A and point B conditions are shown Figs. 9(a) and 9(b), respectively. The chemical potentials of C, N, and F are chosen to avoid the formation of secondary phases such as VN, VC, BiF_3, and VF_3. It is seen that doping of C, N, and F cannot lead to good *p*-type or *n*-type conductivities for $BiVO_4$ because of strong compensation from the intrinsic defects, such as O_{vac} and Bi_{vac}.

3.7 Insights of electronic structure of representative defects

To explicitly address the different electronic natures between deep and shallow defects, the density of states of four representative neutral defects, Mo_V(shallow donor), Cr_V(deep donor), Sr_{Bi}(shallow acceptor) and N_O(deep acceptor) are shown in Fig. 10. The deep defects have their DOS of dopants between the original band gap whereas the DOS of shallow defects is resonant inside the bulk states. Typically, shallow levels have delocalized wavefunctions, whereas deep levels have localized ones. We have plotted the wavefunction squares of above neutral defect states at the Γ points as shown in Figure 11. Fig. 11(a) plots the wavefunction square of the Mo_V defect level. It is seen that the wavefunction associated with the donor level distributes not only around Mo atom, but also around V atoms away from the Mo atom, indicating delocalized feature, which is consistent with the result that Mo_V is a shallow donor. Fig. 11(b) plots the wavefunction square associated with the defect level created by Cr_V. It is seen that the wavefunction is localized around Cr, consistent with the deep level feature. Figure 11(c) plots the wavefunction square associated with the acceptor level created by Sr_{Bi}.. Because the valance band is derived from Bi 6s and O 2p states, the wavefunction is located not only around Sr_{Bi}, but also around Bi and O atoms, indicating that the acceptor is rather shallow. Fig. 11(d) plots the wavefunction square associated with the acceptor level created by N_O,. Because the level created by N_O is not shallow, the wavefunction associated with the N_O level is rather localized.

IV.   Conclusion

We have systematically studied the doping properties of intrinsic and extrinsic defects in $BiVO_4$ using DFT by calculating the transition energies and formation energies of intrinsic and impurity defects and Fermi level pining positions. We found that intrinsic doping can only lead

to moderate *n*-type and *p*-type conductivities at Bi-rich/O-poor and O-rich growth conditions, respectively, though O vacancies are very shallow donors and Bi vacancies are very shallow acceptors. We further found that outstanding *p*-type conductivity can be achieved by Br, Ca, Na, or K doping at O-rich growth conditions because these impurities at Bi sites are shallow acceptors and have rather low formation energies. Excellent *n*-type conductivity can be realized by Mo or W doping at O-poor growth conditions, because they are very shallow donors at V sites and have very low formation energies. The formation energies and transition energies of the defects discussed depend on the atomic size and atomic chemical potential trends.

References

[1]   A. Fujishima and K. Honda, *Nature (London)* **238**, 37 (1972).

[2]   M. D. Hernandez-Alonso, F. Fresno, S. Suarez, and J. M. Coronado, *Energy Environ. Sci.* **2**, 1231 (2009).

[3]   A. Kudo and Y. Miseki, *Chem. Soc. Rev.* **38**, 253 (2009).

[4]   Z. Zou, J. Ye, K. Satama, and H. Arakawa, *Science* **414**, 625 (2001).

[5]   A. Walsh, Y. Yan, M. N. Huda, M. M. Al-Jassim, and S.-H. Wei, *J. Phys. Chem. C* **112**, 12044 (2009).

[6]   A. Walsh, J. L. F. Da Silva, Y. Yan, M. N. Huda, M. M. Al-Jassim, and S.-H. Wei, *Phys. Rev. B* **79**, 073105 (2009).

[7]   L. Kong, H. Y. Chen, W. Hua, S. Zhang, and J. P. Chen, *Chem. Commun.* **38**, 4977 (2008).

[8]   Y. Hosogi, Y. Shimodaira, H. Kato, H. Kobayashi, and A. Kudo, *Chem. Mater.* **20**, 1299 (2008).

[9]   K. Sayama, A. Nomura, T. Arai, T. Sugita, R. Abe, M. Yanagida, T. Oi, Y. Iwasaki, Y. Abe, and H. Sigihara, *J. Phys. Chem. B* **110**, 11352 (2006).

[10] H. Luo, A. H. Mueller, T. M. McCleskey, A. K. Burrel, E. Bauer, and Q. X. Jia, *J. Phys.Chem. C* **112**, 6099 (2008).

[11] A. Kudo, K. Omori, and H. Kato, *J. Am. Chem. Soc.* **121**, 11459 (1999).

[12] A. Walsh, Y. Yan, M. N. Huda, M. M. Al-Jassim, and S.-H. Wei, *Chem. Mater.* **21**, 547 (2009).

[13] M. C. Long, W. M. Cai, and H. J. Kisch, *J. Phys. Chem. C* **112**, 548 (2008).

[14] W. Yao, H. Iwai, and J. Ye, *Dalton Tran.* **11**, 1426 (2008).

[15] W. Yao and J. Ye, *J. Phys. Chem. B* **110**, 11188 (2006).

[16] S. F. Sameera, P. P. Rao, L. S. Kumari, and P. Koshy, *Chem. Lett.* **38**, 1088 (2009).

[17] T. Duraisamy and A. Ramanan, *Solid State Ionics* **120**, 233 (1999).

[18] W. Yao and J. Ye, *Chem. Phys. Lett.* **450**, 370 (2008).

[19] A. Zhang and J. Zhang, *J. Haza.Mater.* **173**, 265 (2010).

[20] Q. Wang, H. Liu, J. Li, J. Yuan, and W. Shangguan, *Catal. Lett.* **131**, 160 (2009).

[21] G. Lei, *Mater. Lett.* **62**, 926 (2008).

[22] X. Zhang, X. Quan, S. Chen, and Y. Zhang, *J. Haza.Mater.* **177**, 914 (2010).

[23] G. Kresse and J. Furthmuller, *Phys. Rev. B* **54**, 11169 (1996); *Comput. Mater. Sci.* **6**, 15 (1996).

[24] P. E. Blochl, *Phys. Rev. B* **50**, 17953 (1994); G. Kresse and D. Joubert, **59**, 1758 (1999).

[25] J. P. Perdew and Y. Wang, *Phys. Rev. B* **45**, 132444 (1992).

[26] S.-H. Wei, *Comp. Mater. Sci.* **30**, 337 (2004).

[27] Y. Yan and S.-H. Wei, *phys. stat. sol. (b)* **4**, 641 (2008).

[28] Y. Yan, J. B. Li, S.-H. Wei, and M. M. Al-Jassim, *Phys. Rev. Lett.* **98**, 135506 (2007).

[29] Y. Yan, M. M. Al-Jassim, and S.-H. Wei, *Appl. Phys. Lett.* **89**, 181912 (2006).

[30] J. Li, S.-H. Wei, S. S. Li, and J. B. Xia, *Phys. Rev. B* **74**, 081201 (2006).

[31] D. J. Payne, R. G. Egdell, A. Walsh, G. W. Watson, J. Guo, P.-A. Glans, T. Learmonth, and K. E. Smith, *Phys. Rev. Lett.* **96**, 157403 (2006).

[32] M. W. Stoltzfus, P. M. Woodward, R. Seshadri, J.-H. Klepeis, and B. Bursten, *Inorg. Chem.* **46**, 3839 (2007).

[33] W.-J. Yin, S.-H. Wei, M. M. Al-Jassim, and Y. Yan, unpublished.

[34] http://boomeria.org/chemlectures/textass2/firstsemass.html

[35] B. R. Li, Y. H. Mo, and X. Z. Wang, Inorganic Dielectric Materials (Shanghai Science and Technology Press, China, 1986), pp. 3-8.

[36] *Zinc Oxide – A Material for Micro and Optoelectronic Applications*, edited by N. H. Nickel and E. Terukov (Springer, Netherland, 2005).

[37] C. H. Park, S. B. Zhang, and S.-H. Wei, *Phys. Rev. B* **66**, 073202 (2002).

[38] E.-C. Lee, Y.-S. Kim, Y.-G. Jin, and K. J. Chang, *Phys. Rev. B* **64**, 085120 (2001).

[39] J. L. Lyons, A. Janotti, and C. G. Van de Walle, *Appl. Phys. Lett.* **95**, 252105 (2009).

[40] W.-J. Yin, H. Tang, S.-H. Wei, M. M. Al-Jassim, J. Turner, and Y. Yan, *Phys. Rev. B* **82**, 045106 (2010).

[41] Y. Gai, J. Li, S.-S. Li, J.-B. Xia, and S.-H. Wei, *Phys. Rev. Lett.* **102**, 036402 (2009).

[42] W. Zhu, X. Qiu, V. Tancu. X.-Q. Chen, H. Pan, W. Wang, N. M. Domitrijevic, T. Rajh, H. M. Meyer III, M. P. Oaranthaman, G. M. Stocks, H. H. Weitering, B. Gu, G. Eres, and Z. Zheng, *Phys. Rev. Lett.* **103**, 226401 (2009).

[43] K.-S. Ahn, Y. Yan. S. Shet, T. Deutsch, J. Turner, and M. Al-Jassim, *Appl. Phys. Lett.* **91** 231909 (2007).

[44] S. Shet, K.-S. Ahn, Y. Yan, T. Deutsch, K. M. Chrustowski, J. Turner, M. Al-Jassim, and N. Ravindra, *J. App. Phys.* **103**, 073504 (2007).

[45] A. E. Rakhshani, Y. Makdisi, and H. A. Ramazaniyan, *J. Appl. Phys.* **83**, 1049 (1998).

[46] D. Li, H. Haneda, N. K. Labhsetwar, S. Hishita, and N. Ohashi, *Chem. Phys. Lett.* **401**, 579 (2005).

Table I. Electron ionization energies of donors and transition energy levels of acceptors (in eV) of intrinsic defects.

Donor	$E_i(0/+1)$	$E_i(0/+2)$	$E_i(0/+3)$	$E_i(0/+4)$	$E_i(0/+5)$
O_{vac}	0.22	-0.17			
V_{Bi}	0.52	0.68			
V_{int}	0.31	0.46	0.56	0.76	0.94
Acceptor	$\varepsilon_i(0/-1)$	$\varepsilon_i(0/-2)$	$\varepsilon_i(0/-3)$	$\varepsilon_i(0/-4)$	$\varepsilon_i(0/-5)$
Bi_{vac}	0.14	0.16	0.18		
V_{vac}	0.23	0.25	0.27	0.30	0.26
Bi_V	1.23	1.15			
O_{int}	0.74	0.49			

Table II. Ionic radii of elements studied in this paper. Values are from Ref. 34 except Bi^{3+}, which is from Ref. 35.

Ions	Radius (Å)	Ions	Radius (Å)
Li^+	0.68	Zr^{4+}	0.79
Na^+	0.95	Hf^{4+}	0.78
K^+	1.33	Cr^{6+}	0.52
Mg^{2+}	0.65	Mo^{6+}	0.62
Zn^{2+}	0.74	W^{6+}	0.65
Ca^{2+}	0.99	Bi^{3+}	1.11
Ti^{4+}	0.68	V^{5+}	0.52

Table III. Electron ionization energies of donors and transition energy levels of acceptors (in eV) in Group I element doping.

Donor	$E_i(0/+1)$	$E_i(0/+2)$	$E_i(0/+3)$	$E_i(0/+4)$
Li_{int}	0.02			
Na_{int}	0.03			
K_{int}	0.04			
Acceptor	$\varepsilon_i(0/-1)$	$\varepsilon_i(0/-2)$	$\varepsilon_i(0/-3)$	$\varepsilon_i(0/-4)$
Li_{Bi}	0.09	0.11		
Li_V	0.22	0.24	0.27	0.29
Na_{Bi}	0.08	0.11		
Na_V	0.23	0.25	0.28	0.30
K_{Bi}	0.16	0.18		
K_V	0.22	0.24	0.27	0.28

Table IV. Electron ionization energies of donors and transition energy levels of acceptors (in eV) in Group II element doping.

Donor	$E_i(0/+1)$	$E_i(0/+2)$	$E_i(0/+3)$
Mg_{int}	0.06	0.12	
Ca_{int}	0.04	0.11	
Sr_{int}	0.04	0.10	
Zn_{int}	0.08	0.15	
Acceptor	$\varepsilon_i(0/-1)$	$\varepsilon_i(0/-2)$	$\varepsilon_i(0/-3)$
Mg_{Bi}	0.02		
Mg_V	0.20	0.22	0.25
Ca_{Bi}	0.08		
Ca_V	0.21	0.24	0.25
Sr_{Bi}	0.09		
Sr_V	0.21	0.25	0.26
Zn_{Bi}	0.02		
Zn_V	0.21	0.24	0.26

Table V. Electron ionization energies of donors and transition energy levels of acceptors (in eV) in Group IVB element doping.

Donor	$E_i(0/+1)$	$E_i(0/+2)$	$E_i(0/+3)$	$E_i(0/+4)$
Ti_{Bi}	0.20			
Ti_{int}	0.20	0.27	0.39	0.50
Zr_{Bi}	0.04			
Zr_{int}	0.10	0.17	0.28	0.40
Hf_{Bi}	0.08			
Hf_{int}	0.05	0.18	0.30	0.40
Acceptor	$\varepsilon_i(0/-1)$	$\varepsilon_i(0/-2)$	$\varepsilon_i(0/-3)$	$\varepsilon_i(0/-4)$
Ti_V	0.15			
Zr_V	0.17			
Hf_V	0.16			

Table VI. Electron ionization energies (in eV) of donors in Group VIB element doping.

Donor	$E_i(0/+1)$	$E_i(0/+2)$	$E_i(0/+3)$	$E_i(0/+4)$	$E_i(0/+5)$	$E_i(0/+6)$
Cr_{Bi}	1.08	0.85	1.16			
Cr_V	0.41					
Cr_{int}	0.70	0.77	1.03	1.08	1.30	1.40
Mo_{Bi}	0.21	0.42	0.57			
Mo_V	0.04					
Mo_{int}	0.67	0.74	0.90	0.95	1.14	1.22
W_{Bi}	0.09	0.16	0.23			
W_V	0.01					
W_{int}	0.50	0.55	0.68	0.72	0.88	0.93

Table VII. The electron ionization energies of donors and the transition energy levels of acceptors (in eV) in C, N and F doping.

Donor	$E_i(0/+1)$	$E_i(0/+2)$
F_O	0.09	
Acceptor	$\varepsilon_i(0/-1)$	$\varepsilon_i(0/-2)$
N_O	0.26	
C_O	1.02	1.05
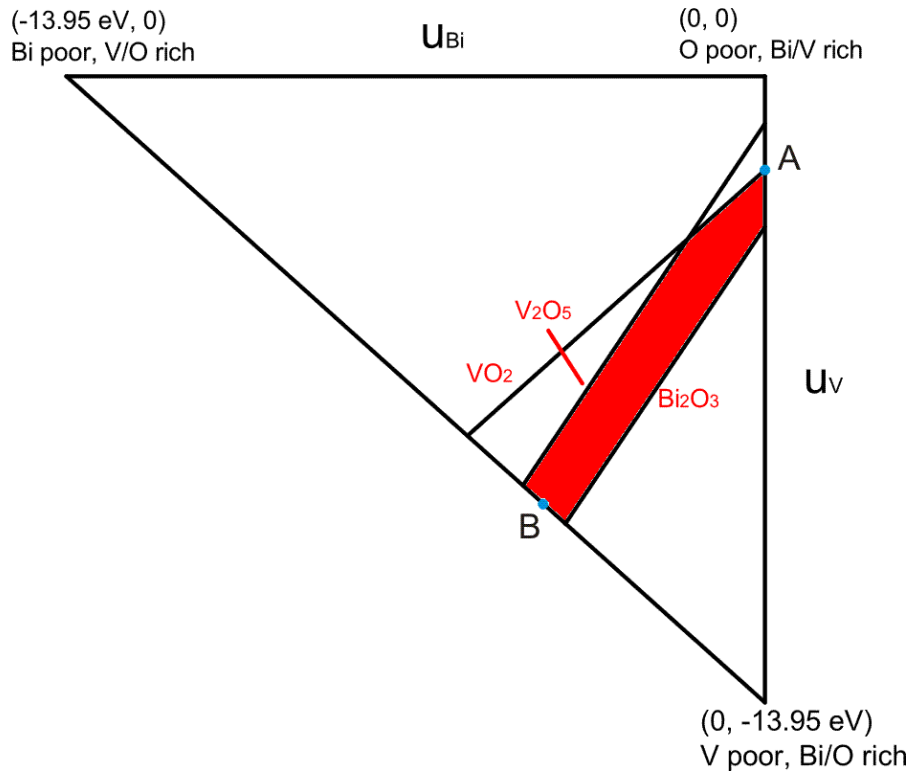
Figure 1: (color online) Accessible range of chemical potentials (red/shadow region) for equilibrium growth condition of BiVO$_4$. Specific points A and B are chosen as the representative chemical potentials for the following defect formation energy calculation, in which the A condition is Bi rich/O poor and the B condition is O rich.
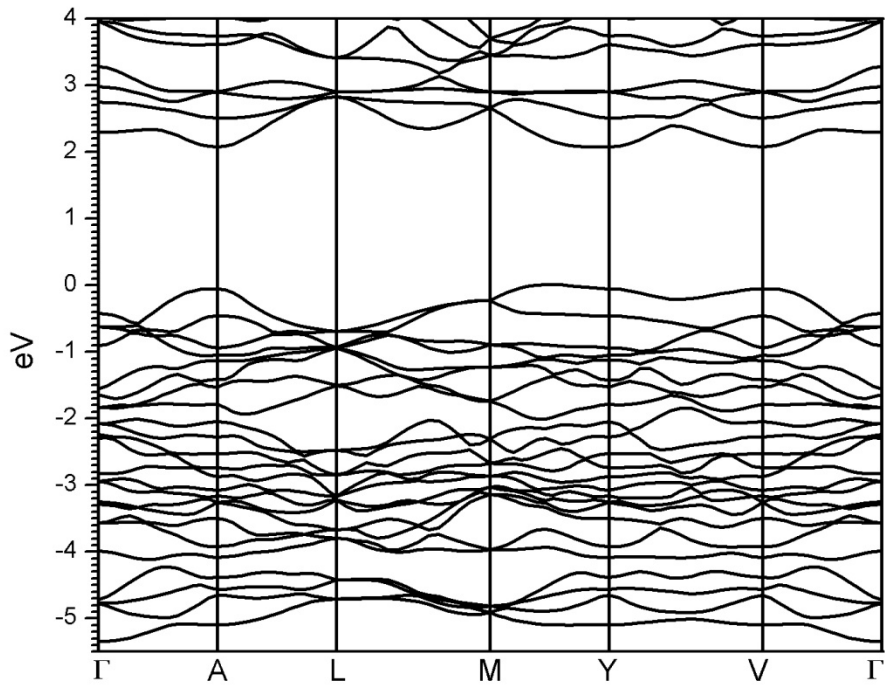
Figure 2: Band structures of BiVO$_4$.
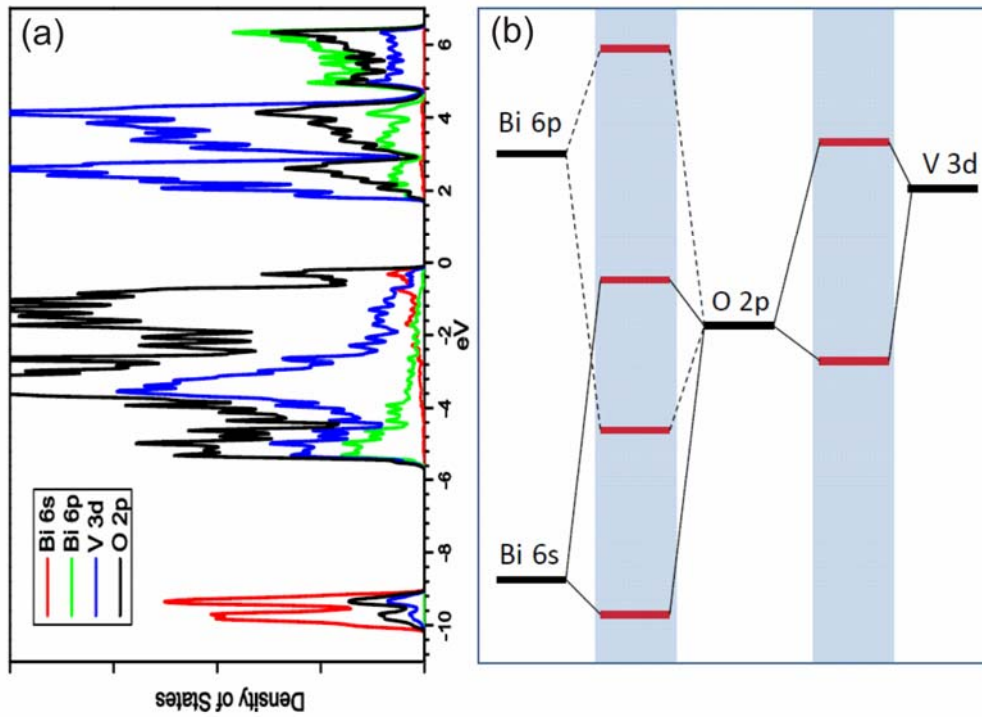
Figure 3: (color online) (a) Partial density of states of bulk $BiVO_4$ and (b) schematic coupling between the main valence states for energy-band formation, where the bonding and antibonding states are formed in shaded region through the coupling of atomic energy levels. The position of energy levels in the shaded region of (b) correspond to states in (a).
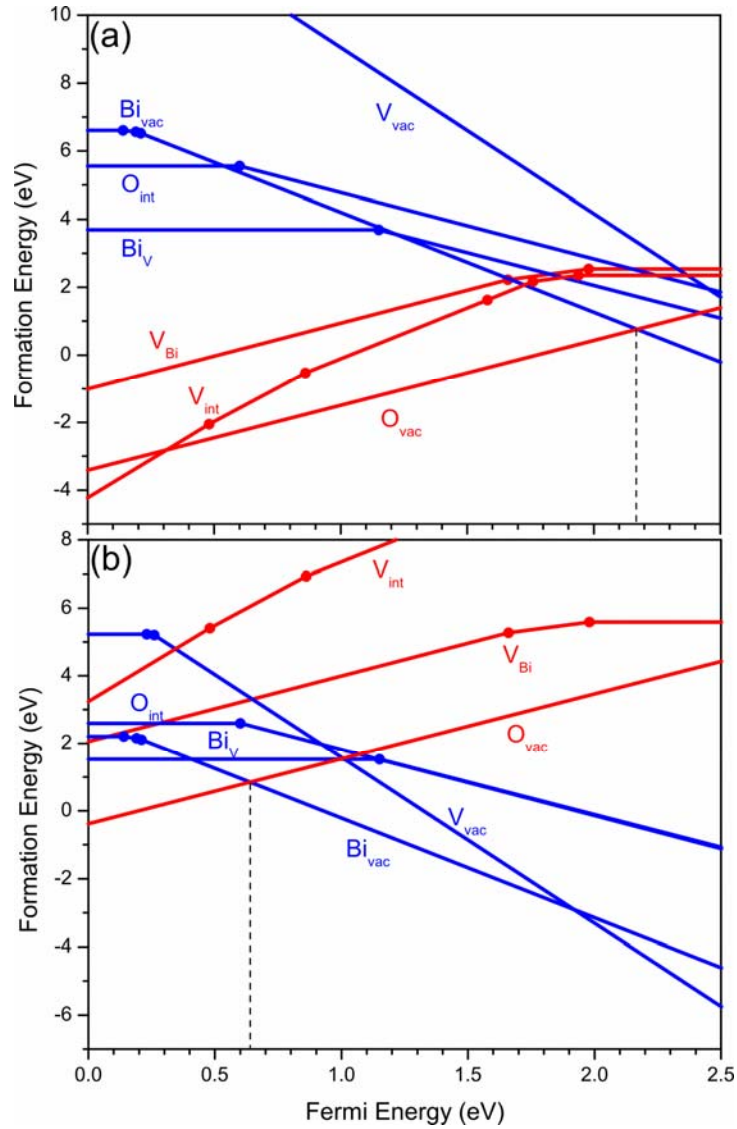
Figure 4: (color online) Formation energies of intrinsic defects Bi_{vac}, V_{vac}, O_{vac}, Bi_V, V_{Bi}, O_{int}, and V_{int} in (a) A (Bi rich/O poor) and (b) B (O rich) conditions. The Fermi level pinnings are indicated by vertical dashed lines.
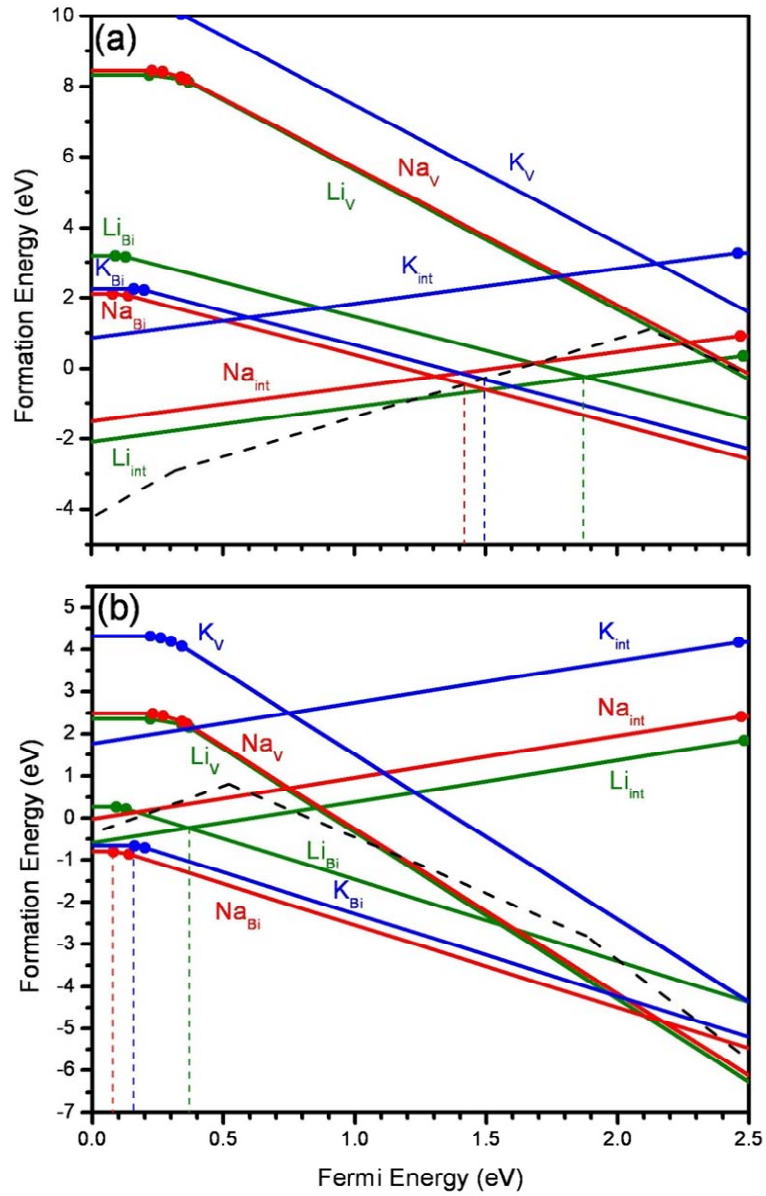
Figure 5: (color online) Formation energies of Li, Na, and K impurities in (a) A (Bi rich/O poor) and (b) B (O rich) conditions. The Fermi level pinnings are indicated by vertical dashed lines.
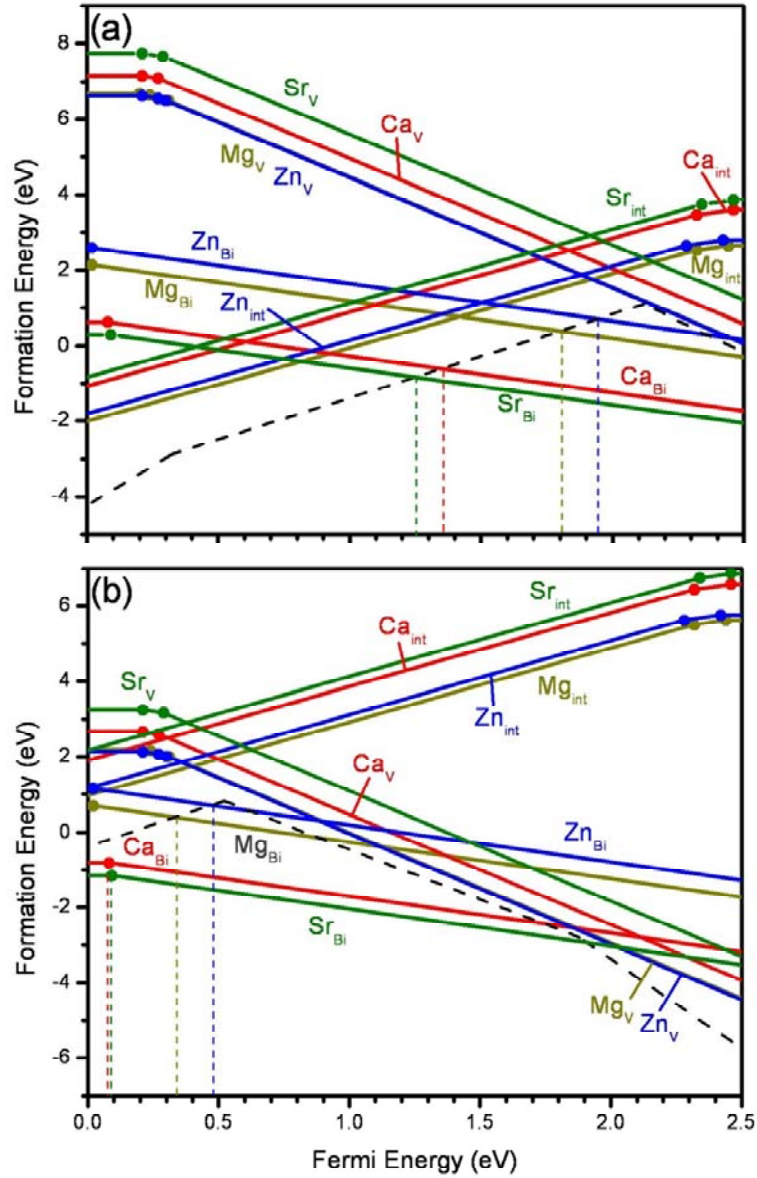
Figure 6: (color online) Formation energies of Mg, Zn, and Ca impurities in (a) A (Bi rich/O poor) and (b) B (O rich) conditions. The Fermi level pinnings are indicated by vertical dashed lines.
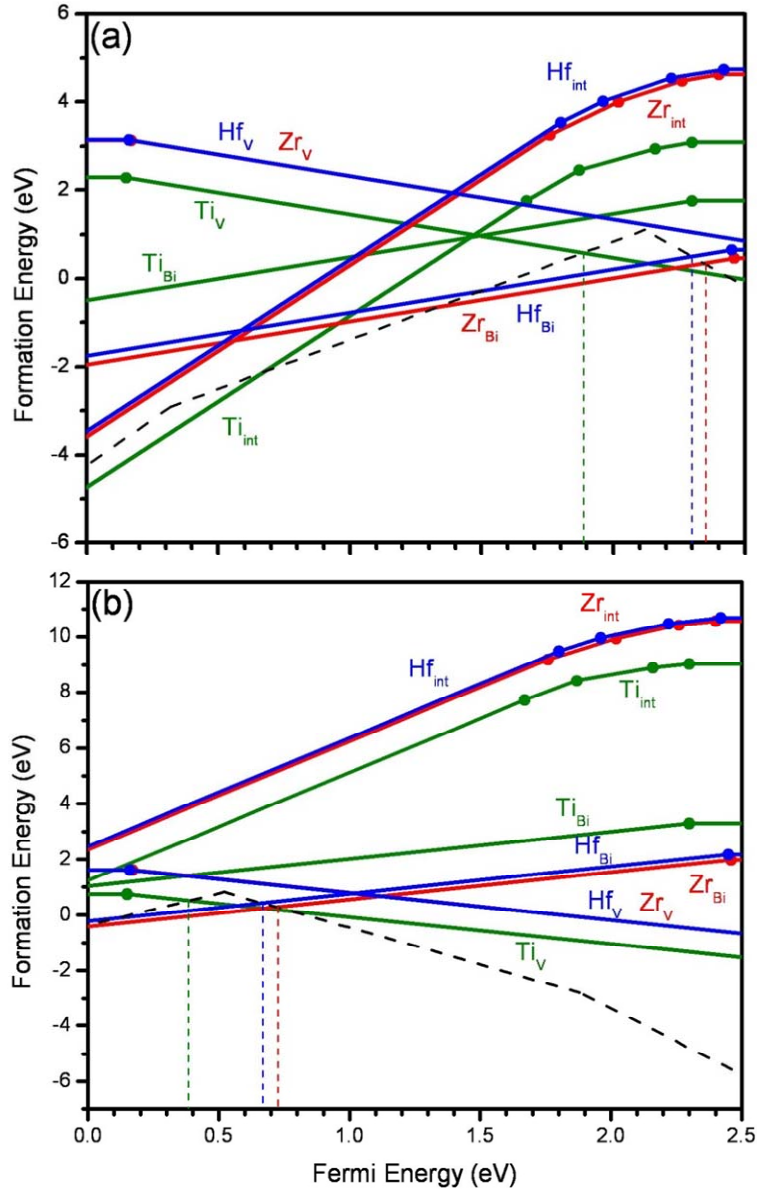
Figure 7: (color online) Formation energies of Ti, Zr, and Hf impurities in (a) A (Bi rich/O poor) and (b) B (O rich) conditions. The Fermi level pinnings are indicated by vertical dashed lines.
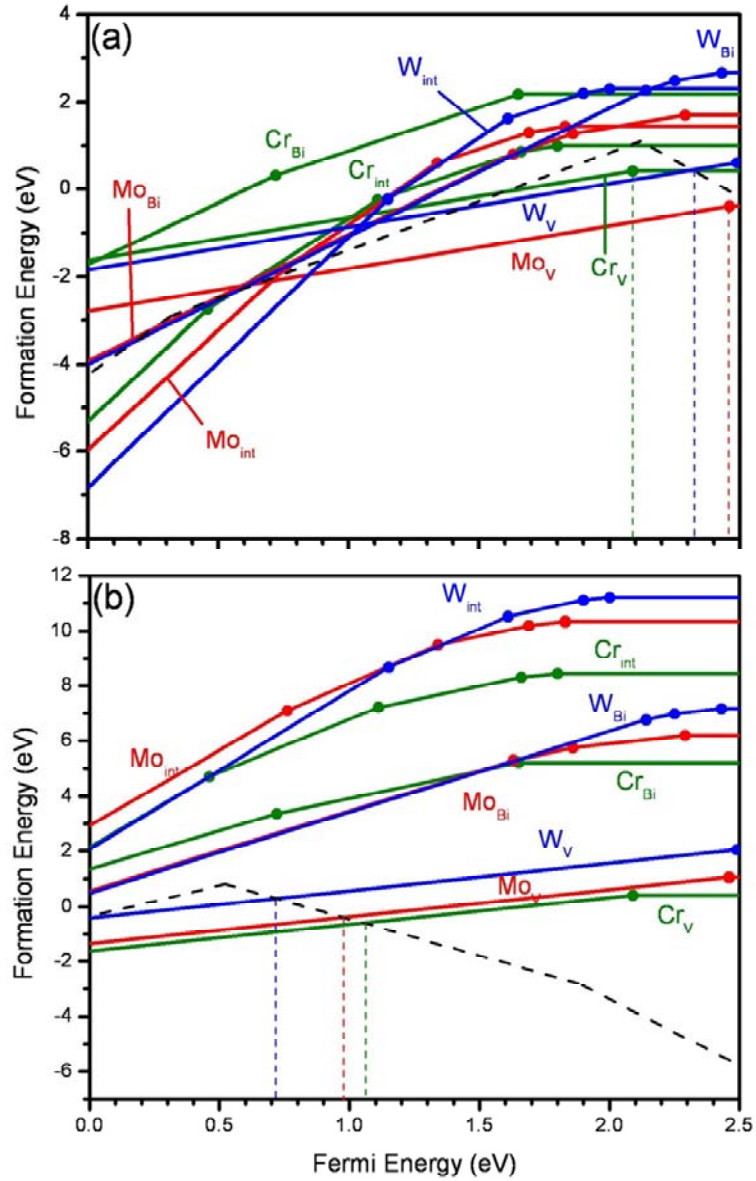
Figure 8: (color online) Formation energies of Cr, Mo, and W impurities in (a) A (Bi rich/O poor) and (b) B (O rich) conditions. The Fermi level pinnings are indicated by vertical dashed lines.
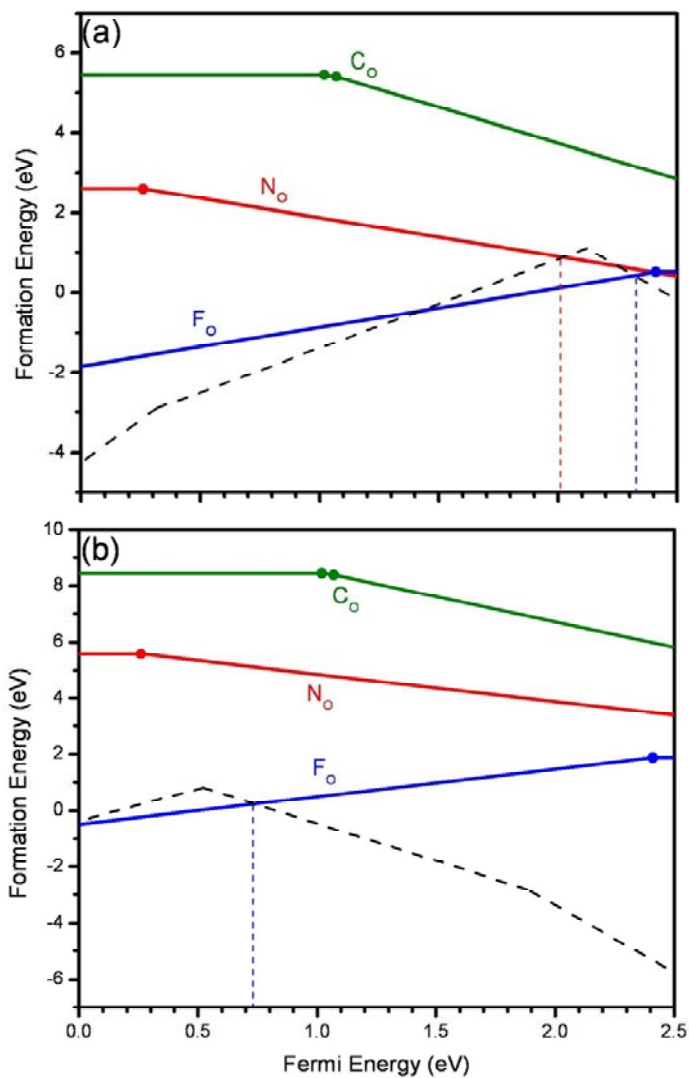
Figure 9: (color online) Formation energies of C_O, N_O, and F_O impurities in (a) A (Bi rich/O poor) and (b) B (O rich) conditions. The Fermi level pinnings are indicated by vertical dashed lines.
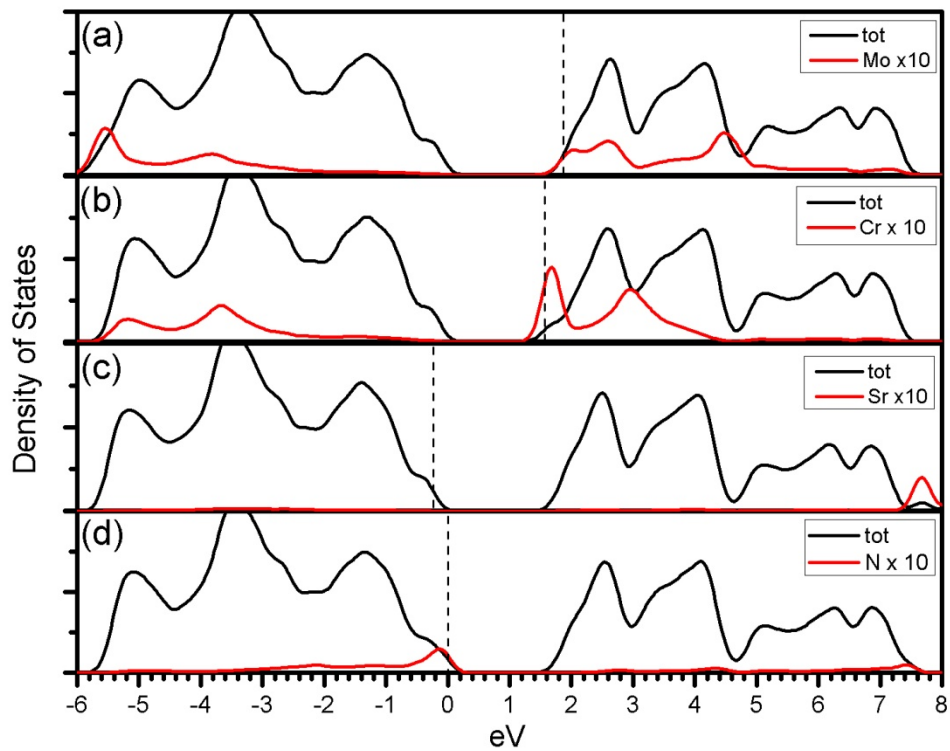
Fig. 10: Density of states (DOS) of the $BiVO_4$ system with dopants (a) Mo_V, (b) Cr_V, (c) Sr_{Bi}, and (d) N_O. The partial DOS on each dopant are enlarged by 10 times for clarity and the dashed lines are Fermi levels in each case.
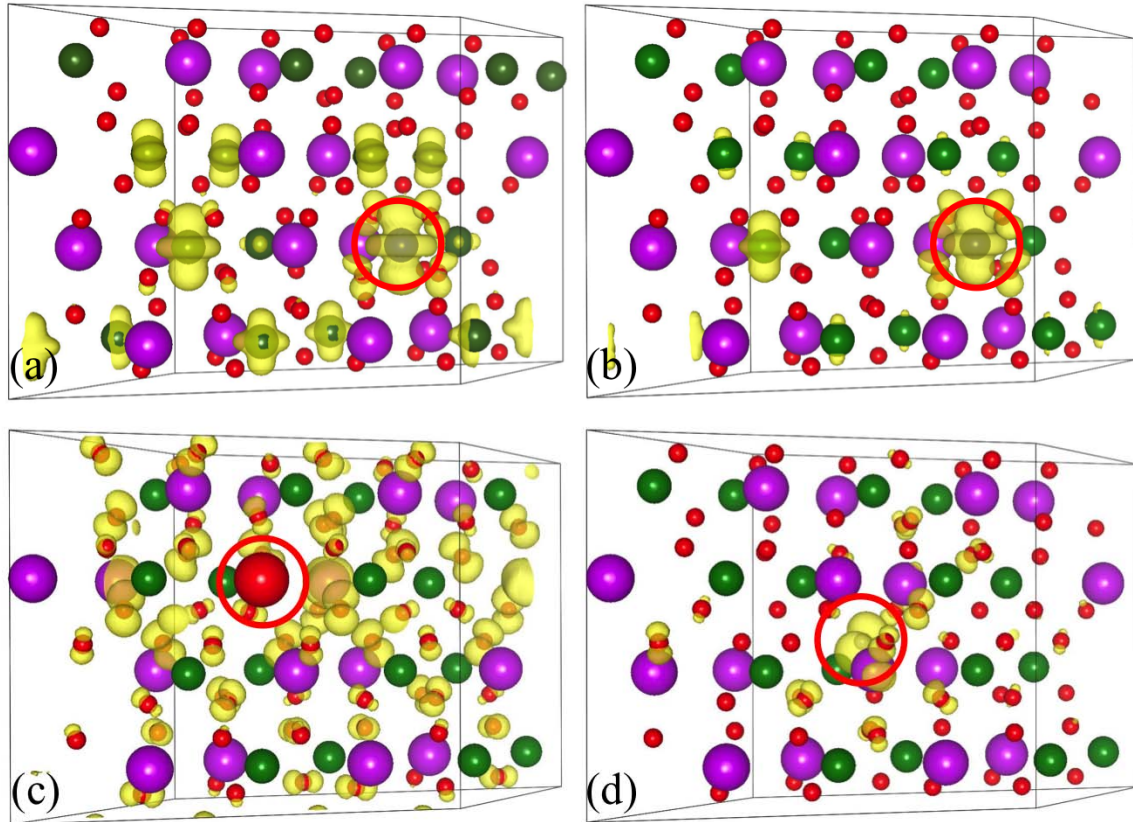
Fig. 11 (color online) Wavefunction squares of the defect levels created by (a) Mo_V, (b) Cr_V, (c) Sr_{Bi}, and (d) N_O. The positions of dopants are marked by circles.